CHEMISTRY
AN ASIAN JOURNAL

DOI: 10.1002/asia.200600111

Microwave-Assisted Synthesis of a Superparamagnetic Surface-Functionalized Porous Fe_3O_4/C Nanocomposite

Xianluo Hu and Jimmy C. Yu*[a]

Abstract: An Fe_3O_4/C nanocomposite was synthesized in a microwave-assisted hydrothermal reaction. This green wet-chemical approach is simple, low-cost, and ideal for large-scale production. The resulting composite material was characterized by transmission electron microscopy, powder X-ray diffraction, energy-dispersive X-ray spectroscopy, Brunauer–Emmett–Teller analysis, X-ray photoelectron spectroscopy, vibrating sample magnetometry, and UV/Vis spectroscopy. The product possesses porous structures and exhibits superparamagnetic behavior. Interestingly, its functional groups were inherited from the starting materials. This hydrophilic and biocompatible nanocomposite may find applications in catalysis, separation, adsorption, and bionanotechnology.

Keywords: hydrothermal synthesis · iron oxide · microwave heating · nanostructures · superparamagnetism

Introduction

Recent advances in the field of novel functional materials are paving the way for exciting applications in modern science and technology.[1] In particular, the general class of inorganic nanocomposite materials is a fast-growing area of chemical research.[2] Considerable effort has been made to design, construct, and manipulate nanostructure composites through innovative synthetic approaches. Nanocomposite materials not only inherit the properties of their individual parents, but also provide the possibility for enhanced functionality and multifunctional properties, in contrast with their more-limited single-component counterparts.[2] For instance, Co/CdSe nanocomposites were shown to retain bifunctional magnetic–optical properties, thus permitting potential applications such as optical "reporters" coupled with magnetic "handles" for use in bioassays.[3] Composite Fe_2O_3/MgO and Fe_2O_3/CaO nanoparticles have greatly enhanced efficiencies over pure MgO and CaO catalysts for SO_2 adsorption, H_2S removal, and chlorocarbon destruction.[4] Recently, our group produced a series of TiO_2-based nanocomposite photocatalysts (e.g., CdS/TiO_2, Pt/TiO_2, and S/TiO_2) that show enhanced catalytic/photocatalytic activities.[5–7] Advances in physical methods have led to an understanding of structure–performance relationships at the molecular level that are strongly related to size, composition, and structural order.[8,9] This knowledge, together with effective strategies for nanostructure construction, has inspired the design and development of new composites for advanced applications.

Hydrothermal/solvothermal synthesis is a well-established approach for producing many inorganic materials with desired micro- or nanostructures.[10] Under closed high-pressure conditions, water or solvents typically exhibit unusual properties, including sufficient density to dissolve materials and high diffusivity to facilitate mass transport.[11] Hydrothermal/solvothermal processing allows many inorganic materials to be synthesized at temperatures substantially lower than those required by conventional solid-state or vapor reactions.[10] In comparison to coprecipitation and sol-gel methods that also allow for relatively low reaction temperatures, hydrothermal/solvothermal processes always give rise to crystalline products without any further postannealing treatment (e.g., calcination after sol-gel processes).[5] However, conventional heating methods in hydrothermal/solvothermal processes often rely on thermal conduction of black-body radiation to drive chemical reactions. They inevitably suffer from several disadvantages, especially at low temperatures, including sharp thermal gradients throughout the bulk solution, slow reaction kinetics, and nonuniform reaction conditions.[12] New approaches have been sought particularly for the controlled growth of nanomaterials, for

[a] X. Hu, Prof. Dr. J. C. Yu
Environmental Science Programme and
The Center of Novel Functional Molecules
Department of Chemistry
The Chinese University of Hong Kong
Shatin, New Territories, Hong Kong (China)
Fax: (+852) 2603-5057
E-mail: jimyu@cuhk.edu.hk

which uniform nucleation and growth rates are critical to material quality. Microwave dielectric heating can address the problems of heating inhomogeneity and slow reaction kinetics, while providing a platform for large-scale industrial applications.[12] The application of this technique is a fast-growing research area of immense potential.[12,13] Microwave heating opens up the possibility of reactions that proceed in a very short time with higher selectivity and energy efficiency compared to conventional heating.[14,15] Very recently, we developed the microwave-enhanced hydrothermal approach for producing carbon-based interconnected cablelike Ag/C and spherical Se/C nanocomposites by taking advantage of microwave heating and hydrothermal effects at a relatively low and controllable temperature.[16] Herein, we report on an extension of this efficient wet-chemical approach to the synthesis of a new functionalized Fe_3O_4/C nanocomposite.

Iron oxide (Fe_2O_3 and Fe_3O_4) nanocrystals have been of much scientific and technological interest over the past decades.[17,18] Their magnetic behavior is exploited for magnetic recording and diverse biomedical applications, including assays,[19] imaging,[20] and drug delivery.[21] So far, a number of synthetic techniques such as coprecipitation, microemulsion, ultrasound irradiation, laser pyrolysis, and thermal decomposition have been developed for producing superparamagnetic nanoparticles.[22] These pure-phase magnetic particles, however, have severe limitations. For example, they tend to aggregate because of strong magnetic attractions between particles with large specific surface areas, and they are prone to biodegradation by microbial attack during their exposure to biological systems.[23] Therefore, chemical modifications must be made to enhance the applicability of nanoscale iron oxide materials. Fe_3O_4 nanoparticles modified by polymers, semiconductors, and metals have been reported.[24] Nanocrystals of iron oxides have also been incorporated into various porous matrices, including silica xerogels/aerogels,[25] nanochannel alumina,[26] mesoporous silicates,[27] aluminosilicates,[28] and carbon materials.[29] Despite these advances, however, challenges still remain in achieving the ideal functionalities of Fe_3O_4-based nanocomposites through a simple but efficient approach. Herein, a nanostructured Fe_3O_4/C composite was synthesized on a large scale through a mild microwave-enhanced hydrothermal route by using starch as a carbonaceous source and water as an environmentally friendly solvent. From the view of green chemistry, this method is favorable as neither hazardous organic solvents nor expensive substances are used, and is therefore ideal for large-scale industrial production. Also, the resulting Fe_3O_4/C nanocomposite contains functionalized hydrophilic and biocompatible surfaces and porous structures, and exhibits superparamagnetic behavior. To the best of our knowledge, this is the first report on a rapid microwave-enhanced hydrothermal synthesis of the functionalized Fe_3O_4/C nanocomposite. Our approach offers several important advantages for the technical application of nanocomposites. First, carbon exhibits high-temperature and high-pressure stability and resists attacks from acids, bases, and solvents.[30,31] Our carbon-modified Fe_3O_4 porous composite is therefore much more stable than pure Fe_3O_4 at the ambient pH values and temperatures found in biological systems. Second, the Fe_3O_4/C composite has great potential in biochemical and medical applications because it can be further conjugated to substances such as antibodies and enzymes. Such potential has been demonstrated recently for a silica-coated Fe_3O_4 system.[23] Third, the nanocomposite is superparamagnetic, which means that it can be manipulated by an external magnetic field. We believe that this biocompatible, superparamagnetic Fe_3O_4/C nanocomposite material may find potential uses in catalysis, separation, adsorption, and bionanotechnology.

Abstract in Chinese:

采用微波輔助的水熱反應法合成了 Fe_3O_4/C 納米複合物。這是一種簡易的、低成本、環境友好的濕化學合成法，適用于規模化生產。分析結果表明所制備的複合物具有多孔結構和超順磁性，表面含有功能基團。這種親水性、生物兼容性的複合物在催化、分離、吸附和生物納米技術等領域具有應用前景。

Results and Discussion

Preliminary attempts to determine the crystalline phase, crystallinity, and particle size of the Fe_3O_4/C nanocomposite were performed by XRD. Figure 1 shows a typical XRD pattern of the product obtained after microwave heating at 200 °C for 30 min. All the reflections can be readily indexed to the spinel phase of Fe_3O_4 (space group: *Fd*3*m* (No. 227)). The calculated lattice constant of $a = 8.40$ Å is in good agreement with the value from the literature ($a = 8.394$ Å; JCPDS no. 75-1610). The broadening of the XRD peaks reflects the nanocrystalline nature of the material. On the basis of a Scherrer analysis of diffraction peak widths for 311 peak common to magnetite, the calculated particle size is around 6.5 nm. Energy-dispersive X-ray (EDX) spectrometry was also used to determine the local chemical composition of the resulting samples. A typical EDX spectrum is shown in Figure 2. Three major peaks correspond to the ele-

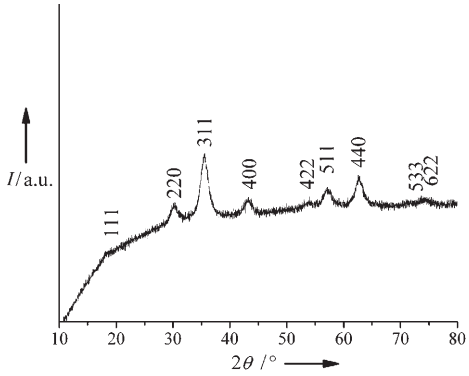

Figure 1. Typical XRD pattern of the Fe_3O_4/C nanocomposite.

CHEMISTRY
AN ASIAN JOURNAL

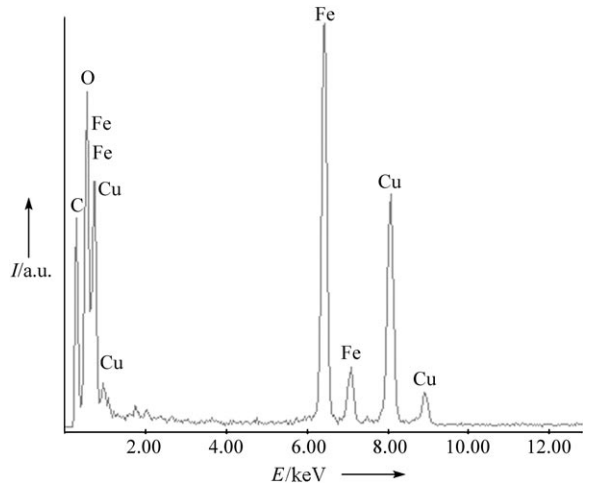

Figure 2. Typical EDX spectrum of the Fe_3O_4/C nanocomposite.

ments C, O, and Fe. The above XRD and EDX results confirm that the composite comprises nanocrystalline Fe_3O_4 and amorphous C.

Transmission electron microscopy (TEM) was used to examine further the crystallinity, particle size, and morphology of the products. Figure 3a shows a typical bright-field TEM image for the product whose XRD pattern is shown in Figure 1. The dark/light contrast is clearly observed. The light patches suggest the existence of numerous nanosized pores with diameters less than 10 nm. These irregular pore structures are connected randomly and lack discernible long-range order in the pore arrangement among the small nanocrystalline Fe_3O_4 particles. The amorphous carbon

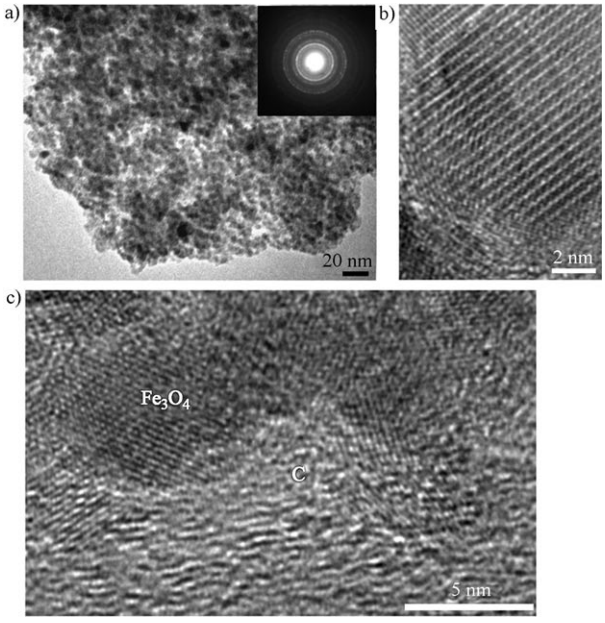

Figure 3. a) Representative TEM image of the Fe_3O_4/C nanocomposite. Inset: SAED pattern indicating the crystalline spinel nature of Fe_3O_4. b) HRTEM image of the (111) lattice fringes of Fe_3O_4. c) HRTEM image of the interface between Fe_3O_4 and C.

cannot be clearly identified in this low-magnification TEM image. The dark patches show that the product comprises an analogous aerogel framework of Fe_3O_4 nanocrystals several nanometers in size. Given the size distribution of Fe_3O_4, the average diameter of the magnetite nanocrystals from the TEM observations agrees well with that obtained from applying the Scherrer formula to the XRD measurements. The corresponding selected-area electron diffraction (SAED) pattern (Figure 3a, inset) reveals diffraction rings of the typical spinel structure of Fe_3O_4, which is also consistent with the XRD result. The high-resolution TEM (HRTEM) image (Figure 3b) shows that the Fe_3O_4 nanoparticles are structurally uniform and crystalline. The interplanar spacing of about 0.48 nm, as indicated clearly by the atomic lattice fringes, corresponds to the (111) lattice planes of cubic Fe_3O_4. Figure 3c shows an HRTEM image of the interface between Fe_3O_4 and carbon. The carbonaceous material serves as a "linker" to bind the iron oxide nanocrystals together. The porous nature of the product comes from the packing of these Fe_3O_4/C nanocomposite particles.

The surface electronic states and the chemical composition of the Fe_3O_4/C nanocomposite were examined by X-ray photoelectron spectroscopy (XPS). The typical wide XPS spectrum of the Fe_3O_4/C nanocomposite in Figure 4a suggests the existence of Fe, O, and C in the product. Both Fe 2p and C 1s peaks were further examined by high-resolution XPS. As shown in the inset of Figure 4a, the peaks at 711.1 and 724.7 eV are the characteristic doublet of Fe $2p_{3/2}$ and Fe $2p_{1/2}$ for iron oxide.[32] In the high-resolution XPS spectrum of the C 1s region (Figure 4b), the peak at 284.6 eV is assigned to the C–C bonds, whereas those at 285.8 and 288.2 eV suggest the existence of functional groups such as OH and C=O.[32] These peaks are mainly attributed to the activated carbonaceous materials (C–C bonds) and partially dehydrated residues from starch (functional groups). The residues containing OH and C=O groups are possibly either covalently bonded or physically anchored to the surface of the Fe_3O_4/C nanocomposite. In this regard, the surface properties of such an Fe_3O_4/C nanocomposite should be greatly

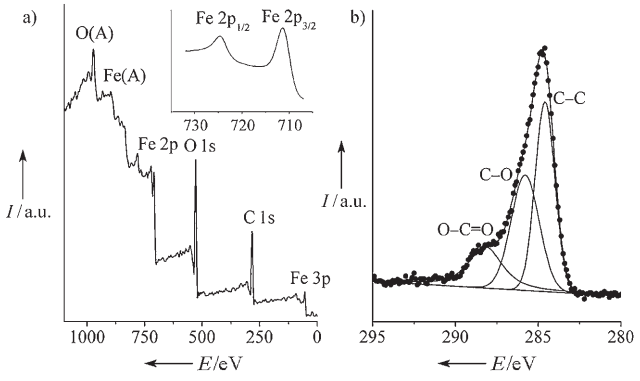

Figure 4. a) Wide-range XPS spectrum of the Fe_3O_4/C nanocomposite. Inset: corresponding high-resolution XPS spectrum for Fe 2p. b) Corresponding high-resolution XPS spectrum for C 1s.

altered and improved. To examine the colloidal stability of the product, the nanocomposite (15 mg) was dispersed in deionized (DI) water (60 mL) under ultrasonication for 10 min and then vigorously stirred for 2 h. The composite particles remained in suspension after being left to stand for several days, thus indicating that they can be well-dispersed in aqueous solution. We believe that this Fe_3O_4/C nanocomposite with enhanced hydrophilicity and stability in an aqueous system may be potentially useful in bionanotechnology. Many unique properties of colloidal particles are based on the functions of the microstructures. They depend greatly on the size, shape, and structure of the building blocks.[8] More recently, Sun and Li[31] reported the synthesis of carbonaceous microspheres from saccharide starting materials by dehydration under conventional hydrothermal conditions. Those microspheres were hydrophilic and functionalized with OH and C=O groups, a result very similar to ours. Furthermore, the thermal and nonthermal effects that are induced by microwave irradiation in our approach probably contribute to the final morphology and structure of the products.[14] Unlike conventional hydrothermal heating, "hot surfaces" on solid Fe_3O_4 as well as "hot spots" may be created by microwave irradiation. These local effects may not only accelerate the dehydration reaction of starch but also improve the crystallinity and magnetization intensity of Fe_3O_4.

In our Brunauer–Emmett–Teller (BET) surface-area analysis, the Fe_3O_4/C nanocomposite exhibits a high surface area ($\approx$79.6 m^2g^{-1}) that is larger than that of bare Fe_3O_4 nanoparticles ($\approx$42.5 m^2g^{-1}) obtained in the absence of starch. This indicates that Fe_3O_4/C is porous whereas the bare Fe_3O_4 is made of solid powder.[33] Figure 5 shows representative nitrogen adsorption–desorption isotherms of Fe_3O_4/C. The inset shows the corresponding pore size distribution curve calculated from the desorption branch of a nitrogen isotherm by the Barrett–Joyner–Halenda (BJH) method with the Halsey equation.[34] In agreement with the direct TEM observations, the type IV and the BJH pore size distribution curves indicate that the Fe_3O_4/C nanocomposite contains micropores (<2 nm) and mesopores with a maximum pore diameter of about 10 nm. Such a porous nanocomposite with high surface area is advantageous for applications that require rapid mass transport or pore accessibility to larger molecules.[6]

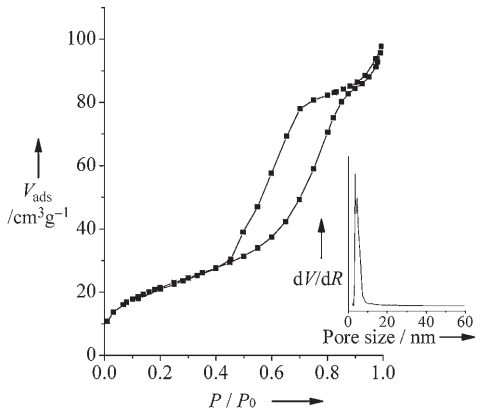

Figure 5. Nitrogen adsorption–desorption isotherms for the Fe_3O_4/C nanocomposite. The inset shows the corresponding BJH pore-size distribution.

The magnetic properties of the Fe_3O_4/C nanocomposites were investigated with a vibrating sample magnetometer (VSM). Figure 6a shows a representative magnetic hysteresis loop of Fe_3O_4/C measured at room temperature, which suggests typical superparamagnetic behavior with zero coercivity and remanence.[18] Even with large aggregates, the porous composite showed no remanence when the magnetic field was removed, which suggests that the individual Fe_3O_4 nanocrystals in the composite is noninteracting. This superparamagnetism is very useful in technical applications such as magnetic separation. Figure 6b displays the temperature-dependence magnetization curves measured at a magnetic

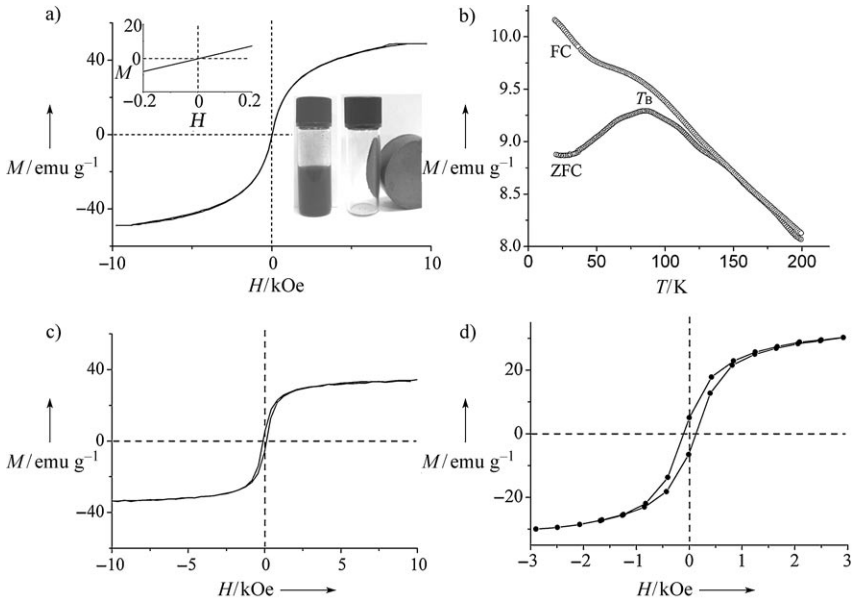

Figure 6. a) Hysteresis loop of the Fe_3O_4/C composite determined at room temperature. Upper-left inset: magnified M versus H curve at low magnetic field (−0.2 to 0.2 kOe) showing the superparamagnetic behavior (zero coercivity and remanence). Lower-right inset: photographs of aqueous Fe_3O_4/C suspension (5 g L^{-1}) and composite Fe_3O_4/C particles attracted to a magnet. b) Temperature-dependent magnetization (ZFC/FC) of the Fe_3O_4/C composite measured at a magnetic field of 500 Oe, showing a T_B of 85 K. c) Magnetic hysteresis loop of the Fe_3O_4/C composite measured at 10 K. d) Magnified part of c) (−3 to 3 kOe) showing a coercivity force of 130 Oe.

field of 500 Oe. The zero-field cooling (ZFC) and field cooling (FC) measurements gave an estimated blocking temperature (T_B) of 85 K. Figure 6c shows the magnetic hysteresis loop for the Fe_3O_4/C nanocomposite measured at 10 K cooled in the ZFC mode. The corresponding amplification of the loop in the low-field region is shown in Figure 6d. It is clear that the nanocomposite is ferromagnetic at 10 K (below T_B) with a coercivity force of 130 Oe.

The porous Fe_3O_4/C nanocomposite with functionalized hydrophilic and biocompatible surfaces and superparamagnetic behavior may serve as an ideal matrix for studying entrapped biomolecules. As a preliminary study, we immobilized the hemoglobin (Hb) enzyme in the functionalized architecture. Hb is a well-characterized protein with many practical applications.[35] Heme absorption is a very useful conformational probe for studying heme proteins, and the absorption positions of the Soret adsorption band provide information on the environment of the heme.[35] As shown in Figure 7, Hb–Fe_3O_4/C gives a heme band at 407 nm,

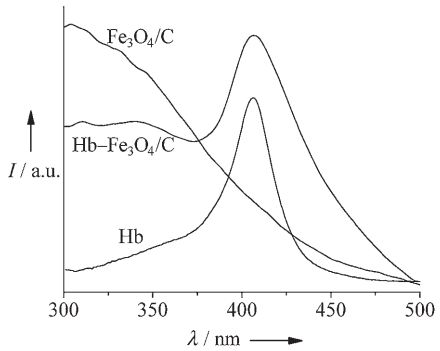

Figure 7. UV/Vis spectra of free Hb and composite Hb–Fe_3O_4/C and Fe_3O_4/C.

which is close to the Soret band at 406 nm for native Hb in the buffer. This indicates that there exists a slight structural variation in the vicinity of the heme site, but no significant denaturation occurs in the porous Fe_3O_4/C composite.[35] A detailed investigation of the binding mechanism is in progress.

Conclusions

We have successfully constructed an Fe_3O_4/C nanocomposite on a large scale through a mild microwave-enhanced hydrothermal approach. This green wet-chemical route is simple and low-cost, and thus is ideal for large-scale industrial production. The Fe_3O_4/C nanocomposite contains porous structures and exhibits superparamagnetic behavior. More importantly, it inherits functional groups from the starting materials. We believe that this hydrophilic and biocompatible nanocomposite will have important applications in catalysis, separation, adsorption, and bionanotechnology.

Experimental Section

Synthesis

All chemicals were of analytical grade and used as received without further purification. In a typical procedure, starch (3 g) was thoroughly dissolved in DI water (20 mL) in a round-bottomed flask at 90 °C, and the flask was then placed immediately in a temperature-controlled water bath at (60 ± 1) °C. After addition of solutions of $FeCl_2$ (5 mL, 0.3 M) and $FeCl_3$ (5 mL, 0.6 M) with vigorous mechanical stirring, aqueous NaOH (1 mL, 15 M) was rapidly injected through a plastic syringe. Argon gas was bubbled through the reaction medium during the coprecipitation process. The reaction and crystal growth were allowed to proceed for 30 min at 60 °C with vigorous stirring. Finally, a black-brown suspension was obtained, which was cooled to room temperature and sealed in a double-walled high-pressure digestion vessel. After treatment at 200 °C for 30 min with a microwave digestion system (Ethos TC, Milestone), the vessel was cooled to room temperature. The product was collected, washed with DI water and alcohol, and dried in a vacuum at 40 °C for 4 h (yield ≈ 120 mg). For immobilizing of the Hb molecules, Fe_3O_4/C (40 mg) was mixed with Hb stock solution (6 mL, 4 mg mL^{-1}, pH 7.2, 10 mM potassium phosphate buffer) and stirred for 1 h at room temperature. The composite Hb–Fe_3O_4/C was separated from the suspension by magnetic decantation, washed, and dried at 4 °C for further studies.

Characterization

Powder XRD patterns were recorded on a Bruker D8 Advance diffractometer with high-intensity $Cu_{K\alpha 1}$ irradiation ($\lambda = 1.5406$ Å). Diffraction patterns were collected from 10° to 80° at a rate of 2.4° per minute with a step size of 0.02°. TEM images were recorded on a Tecnai F20 (FEI, 200 kV) microscope and a CM-120 microscope (Philips, 120 kV) coupled with an EDX (Oxford Instrumentys) spectrometer. Samples were deposited on thin amorphous carbon films supported by copper grids from ultrasonically processed solutions of the products in ethanol. A Kratos ASIS-HS X-ray photoelectron spectroscope equipped with a standard monochromatic source ($Al_{K\alpha}$) operating at 150 W (15 kV, 10 mA) was employed for surface analysis. The binding-energy (B. E.) scale was calibrated by determining the B. E. of Au $4f_{7/2}$ (84.0 eV). UV/Vis spectra were collected at room temperature with a Varian Cary 100 UV/Vis Scan spectrometer. The colloidal dispersion (in DI water) was placed in a quartz cuvette, which was gently shaken before the spectrum was recorded. BET surface areas and porosities were determined by nitrogen adsorption and desorption with a Micrometritics ASAP2010 analyzer. All the samples were degassed at 393 K overnight. Powdered products were weighed out for magnetic characterization by vibrating sample magnetometry (VSM-7300, Lakeshore, USA).

Acknowledgements

This work was supported by the Strategic Investments Scheme administrated by The Chinese University of Hong Kong. We thank Dr. Z. Zheng for XPS measurements, Mr. Andrew S. K. Li for exploring the magnetic properties, and Dr. J. M. Gong for helpful discussions. We appreciate the assistance of Prof. Q. Li for TEM measurements.

[1] B. L. Cushing, V. L. Kolesnichenko, C. J. O'Connor, *Chem. Rev.* **2004**, *104*, 3893.
[2] a) P. M. Ajayan, O. Stephan, P. Redlich, C. Colliex, *Nature* **1995**, *375*, 564; b) H. Zeng, J. Li, J. P. Liu, Z. L. Wang, S. H. Sun, *Nature* **2002**, *420*, 395; c) Z. Y. Sun, Z. M. Liu, B. X. Han, Y. Wang, J. M. Du, Z. L. Xie, G. J. Han, *Adv. Mater.* **2005**, *17*, 928.
[3] H. Kim, M. Achermann, L. P. Balet, J. A. Hollingsworth, V. I. Klimov, *J. Am. Chem. Soc.* **2005**, *127*, 544.
[4] a) S. Decker, S. K. J. Klabunde, *J. Am. Chem. Soc.* **1996**, *118*, 12465; b) C. L. Carnes, K. J. Klabunde, *Chem. Mater.* **2002**, *14*, 1806.
[5] J. C. Yu, L. Wu, J. Lin, P. S. Li, Q. Li, *Chem. Commun.* **2003**, 1552.

[6] X. C. Wang, J. C. Yu, H. Y. Yip, L. Wu, P. K. Wong, S. Y. Lai, *Chem. Eur. J.* **2005**, *11*, 2997.
[7] a) J. C. Yu, W. K. Ho, J. G. Yu, H. Yip, P. K. Wong, J. C. Zhao, *Environ. Sci. Technol.* **2005**, *39*, 1175; b) J. C. Yu, X. C. Wang, L. Wu, W. K. Ho, L. Z. Zhang, G. T. Zhou, *Adv. Funct. Mater.* **2004**, *14*, 1178.
[8] P. Jiang, J. F. Bertone, V. L. Colvin, *Science* **2001**, *291*, 453.
[9] a) Y. W. C. Cao, R. C. Jin, C. A. Mirkin, *Science* **2002**, *297*, 1536; b) Y. G. Sun, Y. N. Xia, *Science* **2002**, *298*, 2176; c) Y. Volokitin, J. Sinzig, L. J. de Jongh, G. Schmid, M. N. Vargaftik, I. I. Moiseevi, *Nature* **1996**, *384*, 621.
[10] a) X. Wang, J. Zhuang, Q. Peng, Y. D. Li, *Nature* **2005**, *437*, 121; b) S. H. Feng, R. R. Xu, *Acc. Chem. Res.* **2001**, *34*, 239; c) K. B. Tang, Y. T. Qian, J. H. Zeng, X. G. Yang, *Adv. Mater.* **2003**, *15*, 448; d) Y. Xie, Y. T. Qian, W. Z. Wang, S. Y. Zhang, Y. H. Zhang, *Science* **1996**, *272*, 1926.
[11] M. Siskin, A. R. Katritzky, *Science* **1991**, *254*, 231.
[12] a) S. Komarneni, *Curr. Sci.* **2003**, *85*, 1730; b) F. Gao, Q. Y. Lu, S. Komarneni, *Chem. Mater.* **2005**, *17*, 856; c) B. L. Newalkar, S. Komarneni, H. Katsuki, *Chem. Commun.* **2000**, 2389; d) J. A. Gerbec, D. Magana, A. Washington, G. F. Strouse, *J. Am. Chem. Soc.* **2005**, *127*, 15791.
[13] a) Y. J. Zhu, W. W. Wang, R. J. Qi, X. L. Hu, *Angew. Chem.* **2004**, *116*, 1434; *Angew. Chem. Int. Ed.* **2004**, *43*, 1410; b) Y. J. Zhu, X. L. Hu, *Chem. Lett.* **2004**, *33*, 760; c) Y. J. Zhu, X. L. Hu, *Chem. Lett.* **2003**, *32*, 1140.
[14] M. Tsuji, M. Hashimoto, Y. Nishizawa, M. Kubokawa, T. Tsuji, *Chem. Eur. J.* **2005**, *11*, 440.
[15] a) S. A. Galema, *Chem. Soc. Rev.* **1997**, *26*, 233; b) D. Adam, *Nature* **2003**, *421*, 571.
[16] a) J. C. Yu, X. L. Hu, Q. Li, L. Z. Zhang, *Chem. Commun.* **2005**, 2704; b) J. C. Yu, X. L. Hu, Q. Li, Z. Zheng, Y. M. Xu, *Chem. Eur. J.* **2006**, *12*, 548.
[17] a) C. J. Jia, L. D. Sun, Z. G. Yan, L. P. You, F. Luo, X. D. Han, Y. C. Pang, Z. Zhang, C. H. Yan, *Angew. Chem.* **2005**, *117*, 4402; *Angew. Chem.Int. Ed.* **2005**, *44*, 4328; b) B. L. Frankamp, A. K. Boal, M. T. Muominen, V. M. Rotello, *J. Am. Chem. Soc.* **2005**, *127*, 9731; c) M. Blanco-Mantecon, K. O'Grady, *J. Magn. Magn. Mater.* **1999**, *203*, 50.
[18] S. F. Si, C. H. Li, X. Wang, D. P. Yu, Q. Peng, Y. D. Li, *Cryst. Growth Des.* **2005**, *5*, 391.
[19] H. W. Gu, P. L. Ho, K. W. T. Tsang, L. Wang, B. Xu, *J. Am. Chem. Soc.* **2003**, *125*, 15702.
[20] Z. Li, L. Wei, M. Y. Gao, H. Lei, *Adv. Mater.* **2005**, *17*, 1001.
[21] W. R. Zhao, J. L. Gu, L. X. Zhang, H. R. Chen, J. L. Shi, *J. Am. Chem. Soc.* **2005**, *127*, 8916.
[22] Z. Li, H. Chen, H. B. Bao, M. Y. Gao, *Chem. Mater.* **2004**, *16*, 1391, and references therein.
[23] Y. P. He, S. Q. Wang, C. R. Li, Y. M. Miao, Z. Y. Wu, B. S. Zou, *J. Phys. D: Appl. Phys.* **2005**, *38*, 1342.
[24] a) D. K. Kim, M. Mikhaylova, F. H. Wang, J. Kehr, B. Bjelke, Y. Zhang, T. Tsakalakos, M. Muhammed, *Chem. Mater.* **2003**, *15*, 4343; b) J. Li, H. Zeng, S. H. Sun, J. P. Liu, Z. L. Wang, *J. Phys. Chem. B* **2004**, *108*, 14005; c) H. Yu, M. Chen, P. M. Rice, S. X. Wang, R. L. White, S. H. Sun, *Nano Lett.* **2005**, *5*, 379; d) A. A. Ismail, *Appl. Catal. B* **2005**, *58*, 115.
[25] a) E. M. Moreno, M. Zayat, M. P. Morales, C. J. Serna, A. Roig, D. Levy, *Langmuir* **2002**, *18*, 4972; b) C. Cannas, M. F. Casula, G. Concas, A. Corrias, D. Gatteschi, A. Falqui, A. Musinu, C. Sangregorio, G. Spano, *J. Mater. Chem.* **2001**, *11*, 3180.
[26] S. A. M. Tofail, I. Z. Rahman, M. A. Rahman, D. Sutton, S. B. Newcomb, *J. Magn. Magn. Mater.* **2002**, *242*, 588.
[27] S. T. Wong, J. F. Lee, S. F. Cheng, C. Y. Mou, *Appl. Catal. A* **2000**, *198*, 115.
[28] C. Garcia, Y. Zhang, F. DiSalvo, U. Wiesner, *Angew. Chem.* **2003**, *115*, 1564; *Angew. Chem. Int. Ed.* **2003**, *42*, 1526.
[29] C. Minchev, H. Huwe, T. Tsoncheva, D. Paneva, M. Dimitrov, I. Mitov, M. Fröba, *Microporous Mesoporous Mater.* **2005**, *81*, 333.
[30] A. H. Lu, W. C. Li, N. Matoussevitch, B. Spliethoff, H. Bonnemann, F. Schuth, *Chem. Commun.* **2005**, 98.
[31] X. M. Sun, Y. D. Li, *Angew. Chem.* **2004**, *116*, 607; *Angew. Chem. Int. Ed.* **2004**, *43*, 597.
[32] J. F. Moulder, W. F. Stickle, P. E. Sobol, K. D. Bomben, *Handbook of X-Ray Photoelectron Spectroscopy*, Perkin Elmer, Eden Prairie, **1992**.
[33] J. G. Yu, J. C. Yu, L. Z. Zhang, X. C. Wang, L. Wu, *Chem. Commun.* **2004**, 2414.
[34] K. S. W. Sing, D. H. Everett, R. A. W. Haul, L. Moscou, R. A. Pierotti, J. Rouquerol, T. Siemieniewska, *Pure Appl. Chem.* **1985**, *57*, 603.
[35] a) S. Peng, Q. M. Gao, Q. G. Wang, J. L. Shi, *Chem. Mater.* **2004**, *16*, 2675; b) J. L. Wang, R. W. Larsen, S. J. Moench, J. D. Satterlee, D. L. Rousseau, M. R. Ondrias, *Biochemistry* **1996**, *35*, 453; c) J. M. Gong, X. Q. Lin, *Microchem. J.* **2003**, *75*, 51.

Received: April 13, 2006
Published online: September 5, 2006

